$Cs^+(18\text{-crown-}6)_2e^-$: A 1D Heisenberg Antiferromagnet with Unusual Phase Transitions

Michael J. Wagner,‡ Andrew S. Ichimura, Rui H. Huang, Richard C. Phillips, and James L. Dye*

Department of Chemistry and Center for Fundamental Materials Research, Michigan State University, East Lansing, Michigan 48824

Received: July 28, 1999; In Final Form: December 6, 1999

Crystalline $Cs^+(18\text{-crown-}6)_2e^-$ was found to be a linear chain Heisenberg antiferromagnet ($J/k_B = -38.3$ K). It undergoes a slow, irreversible transition above ~230 K from a crystalline low temperature (LT) phase to a disordered Curie−Weiss paramagnetic high temperature (HT) phase. A 100 ppm diamagnetic (more shielded) shift of the ^{133}Cs MAS NMR peak accompanies this transition. EPR studies confirm the transition and are in accord with the conversion of the known crystal structure to a disordered phase. This HT phase undergoes an additional first-order *reversible* transition upon cooling below ~220 K ($\Delta H = 0.33$ kJ mol^{-1} upon rewarming) accompanied by the formation of two peaks in the ^{133}Cs NMR spectrum. Variable-temperature powder X-ray diffraction confirms the disordered or microcrystalline nature of the HT phase(s).

Introduction

One of the most intriguing examples of the particle/wave duality of the electron is its role as "anion" in *electrides*.[1−12] In electrides, the wave functions of the anionic electrons are concentrated in vacancies similar to those that provide alkali metal anion sites in crystalline *alkalides*. This situation is analogous to the well-known F-center defects in alkali halide crystals, except that in the case of electrides the salt has a *stoichiometric* number of anionic electrons. Electrides are of considerable theoretical as well as experimental interest.[13−17] They have potential as novel electronic and magnetic materials as well as being model systems of confined electron gases. The simplicity of the electronic structure close to the Fermi level and the absence of strong electron−atom interactions may make them good systems for the study of metal−insulator transitions.

The first crystal structure of an electride, $Cs^+(18\text{-crown-}6)_2e^-$ (abbreviated $Cs^+(18C6)_2e^-$), was published more than a dozen years ago.[18] Early studies characterized this electride by NMR, EPR, powder conductivity, optical absorption spectroscopy, and magnetic susceptibility.[19−23] More recent measurements of electrical conductivity,[24,25] EPR,[26,27] and magnetic susceptibility[28] have raised the question of whether the formerly studied polycrystalline (powder) samples had been "doped" with ceside or existed in several structures with drastically different properties. Theoretical interest in electrides as geometrically well-defined "electron lattice gases" makes it important that questions about the true properties of the crystalline material be resolved. This paper presents the magnetic, optical, and thermal properties of electride samples that have the published crystal structure and shows that increasing the temperature results in irreversible conversion to a disordered or microcrystalline phase or phases with drastically altered properties.

Experimental Section

$Cs^+(18C6)_2e^-$ was synthesized by anaerobically dissolving cesium metal in dimethyl ether in the presence of 10−20% excess complexant in a two-compartment "K-cell".[2,29] Addition of a cosolvent (trimethylamine or diethyl ether) and slow solvent removal (1−2 weeks) at constant temperature (190 K) resulted in large (millimeter size) crystals with the same crystal structure as previously published.[18,28,30] Crystals were selected and pulverized under liquid nitrogen to yield high-quality polycrystalline samples, designated as the LT phase. Care was taken to ensure that their temperature never rose above 190 K during subsequent measurements (except when the effect of temperature was being investigated). All sample transfers were performed in nitrogen-filled glovebags in the presence of an open dewar of liquid nitrogen to limit humidity. The purification of materials and the synthetic methods used have been described in detail elsewhere.[2,9,11,29] The magnetic susceptibility data analyzed in this paper were published earlier.[28]

^{133}Cs NMR spectra were obtained at the Max T. Rogers NMR facility at Michigan State University. Measurements were made with a 9.8950 T Varian VXR 400S NMR spectrometer equipped with a 1 kW pulse amplifier. Variable-temperature magic angle spinning (VT-MAS) spectra were obtained with a Varian probe equipped with a pressurized bearing gas cooling system; dry nitrogen was used for both the bearing and drive gases. During loading, the probe head was protected by a nitrogen-filled glovebag that contained an open dewar of liquid nitrogen to reduce humidity. The probe head was precooled to 153 K with a strong stream of cold nitrogen gas. The sample was then loaded directly from a liquid nitrogen storage dewar in the glovebag. This procedure left no visible condensation on the probe or the rotor even on humid days, so that sample spinning was assured. Samples in silicon nitride rotors were found to consistently spin at between 1.5 and 5.5 kHz.

The sample temperature was determined by using the known temperature dependence of the methanol proton spectra[31] obtained through the decoupler channel. Methanol was contained in a capillary tube inserted into a tight-fitting hole drilled through the center of the rotor cap and anchored in a custom-made Kel-F disk in the bottom of the rotor. Thermal equilibrium was verified by waiting 10 min after the thermocouple in the bearing gas stream had equilibrated to the set temperature and by acquiring

* To whom correspondence should be addressed.
‡ Present address: Department of Chemistry, The George Washington University, Washington, DC, 20052.

10.1021/jp992653b CCC: $19.00
Published on Web 01/19/2000

^1H methanol spectra both before and after each ^{133}Cs spectrum. The ^{133}Cs chemical shifts are referenced to the aqueous cesium cation at infinite dilution. For brevity, chemical shift *changes* are designated "paramagnetic" for positive or less shielded and "diamagnetic" for negative or more shielded directions.

Differential scanning calorimetry (DSC) was carried out with a Shimadzu DSC-50 calorimeter equipped with a low-temperature attachment. Samples were hermetically sealed in aluminum pans with a liquid nitrogen cooled press. The calorimeter was setup and run in a nitrogen glovebag and was precooled to 130 K prior to loading. A steady flow of helium gas was maintained in the sample cell prior to and during the measurements.

A Bruker ESP300E electron spin resonance spectrometer (X-band, 9.5 GHz) was used to acquire EPR spectra. Temperature control in the range 4−290 K was maintained with an Oxford Instruments 9000 liquid helium cryostat. The *g* values were determined by measuring the field and microwave frequency with a Bruker ER035M NMR gaussmeter and an EIP model 25B frequency counter, respectively.

Samples for EPR spectroscopy of powders were prepared by pulverizing a small quantity of crystalline $Cs^+(18C6)_2e^-$ for at least 20 min in a mortar and pestle that had been cooled to 77 K by immersion in liquid nitrogen in a nitrogen-filled glovebag. With this method, the temperature of the sample was maintained at or below 100 K and the atmosphere was kept free of moisture and oxygen. The powdered sample (typically 1−2 mg) was transferred to a quartz EPR tube, which was then sealed off under high vacuum ($\sim 10^{-5}$ Torr) while the sample end was immersed in liquid nitrogen.

Typical instrument parameters used to acquire EPR spectra were as follows: modulation amplitude 0.01 G; modulation frequency 1.56 kHz; gain 10^3; time constant 10 μs; microwave power 1−10 μW. Larger samples or increases in gain, microwave power, or modulation amplitude often result in loss of the AFC lock upon passage through resonance. The sweep width was generally between 4 and 10 G, and sweep times up to 5 min were used. It was found, however, that a sweep time of only 40 s for a 4 G sweep or 80 s for a 10 G sweep yielded line shapes that were practically indistinguishable from those obtained with longer scan times.

For single-crystal EPR studies, a crystal approximately 0.3 mm on each edge was placed in a quartz EPR tube and sealed off under high vacuum. The same set of instrument parameters was used to acquire the spectrum of the single crystal with one variation. Despite the small size of the crystal, the unique orientation of the electron spins caused loss of the AFC lock at resonance. The frequency was therefore stabilized with an external cavity, which enabled acquisition of the single-crystal spectra. As a result, the phase of the radiation field shifted with temperature, so that the spectra obtained in this way had a mixture of absorption and dispersion contributions.

EPR signal intensities were determined by double integration of the first-derivative EPR spectra after subtraction of a constant background correction. The saturation and temperature-dependent behaviors of the spin susceptibility were characterized by their corresponding intensities. Prior to measurement of the temperature dependence, the temperature at the sample site in the center of the TE_{102} resonator was calibrated between 4 and 295 K with a Lakeshore model 208 digital thermometer equipped with a DT-450 silicon diode sensor. The sample was allowed to remain at the desired temperature for several minutes to ensure that the sample had come to thermal equilibrium before the spectrum was acquired.

Powder X-ray diffraction spectra were obtained with a Rigaku RU 200B powder X-ray spectrometer with a low-temperature attachment. Samples were run on aluminum holders and loaded in a glovebag directly from liquid nitrogen into the precooled sample chamber.

Thin films for absorbance, conductivity, and thermionic emission studies were prepared by high-vacuum codeposition of cesium and 18-crown-6 in a stoichiometric ratio of 1:2 onto a sapphire substrate at 211 K as previously described.[32−35]

Results and Conclusions

The first ^{133}Cs NMR study of precipitated samples of $Cs^+(18C6)_2e^-$ showed a single peak at temperatures above 225 K; below this temperature, a second peak, paramagnetically shifted by about 20 ppm, appeared.[23] The chemical shifts were found to vary inversely with temperature and this dependence was attributed to a contact paramagnetic shift (Knight shift) due to interaction with the trapped electrons. However, in the earlier work,[23] accurate temperatures were determined for only four of the NMR spectra, two above and two just below the transition. Other temperatures were assigned by extrapolation, on the assumption that the slope of the chemical shift versus the reciprocal of the temperature was constant. This assumption was based on the belief, shown here to be incorrect, that $Cs^+(18C6)_2e^-$ is a Curie paramagnet and that powdered samples have the same structure as crystals. The existence of two chemically nonequivalent peaks below 225 K is an indication of structural alteration since all cesium sites in the crystalline material[18] are chemically and magnetically equivalent.[36] Details of the ^{133}Cs (spin $I = {}^7/_2$) NMR spectra of oriented single crystals of the LT phase and powders of both the LT and the HT phase(s) will be given in a separate publication. The present study confirms that there is only one central peak for the crystalline (LT) phase. The chemical shift of this peak is about 100 ppm more paramagnetic than that found in the previous study of powders, but the temperature dependence is similar. Upon warming the crystalline LT phase above ~230 K, a second peak grows in whose chemical shift is close to that previously observed. Its growth is slow and the rate is temperature dependent. As the new peak of this HT phase grows, the peak due to the LT phase diminishes. The transformation can be made to go completely to the HT phase by waiting for a sufficient period of time. The LT phase does not re-form upon cooling the sample. Rather, as in the previous study,[23] the single HT peak splits into two peaks at ~220 K that are separated by about 20 ppm. This transition from the HT phase to a new phase or phases (designated HT2) is slow during cooling but the reverse process is rapid upon warming. The two new ^{133}Cs NMR peaks are labeled HT2a (less paramagnetic) and HT2b. At low temperatures the ratio of the intensity of peak HT2a to that of HT2b is approximately 2 to 3. Figure 1 shows the spectrum of a sample at 200 K that had been heated briefly to ~250 K to induce partial transition of the LT phase to the HT phase and then cooled to induce the HT to HT2 transition. This sample contains the peaks LT, HT2a, and HT2b. These dramatic changes in the NMR spectra upon heating a polycrystalline sample can be directly correlated with the thermally induced transition from a linear chain antiferromagnet to a Curie paramagnet, observed by static magnetic susceptibility measurements.[28]

The rate of conversion of the LT phase to the HT phase is dependent on the nature of the sample. The transition is faster for crystalline samples that had been finely ground than for the original crystals. The growth is exponential and is strongly dependent on temperature, with an activation energy of about 200 kJ mol^{-1}.

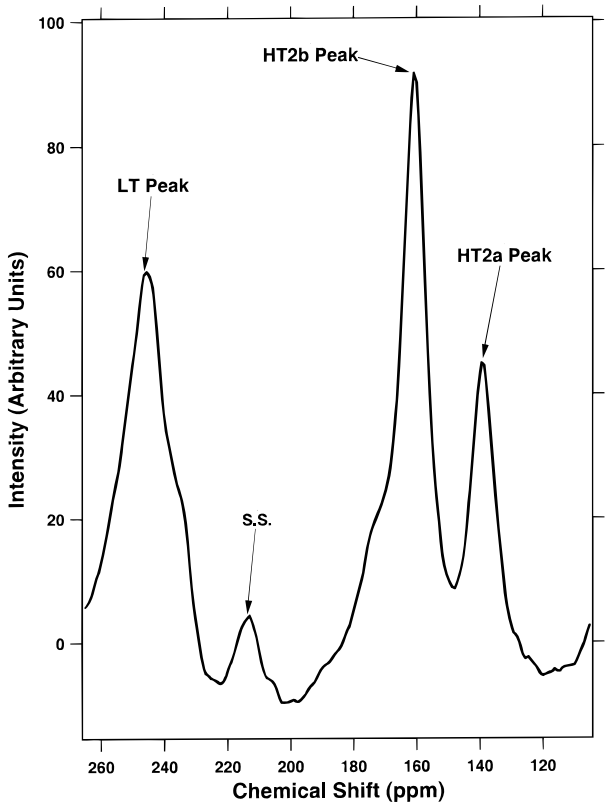

Figure 1. ^{133}Cs MAS NMR spectra after partial transformation from the LT to the HT phase at ~250 K, followed by cooling to ~200 K. This spectrum shows the LT peak and the two peaks of the HT2 phase(s). The peak marked S.S. is a spinning sideband.

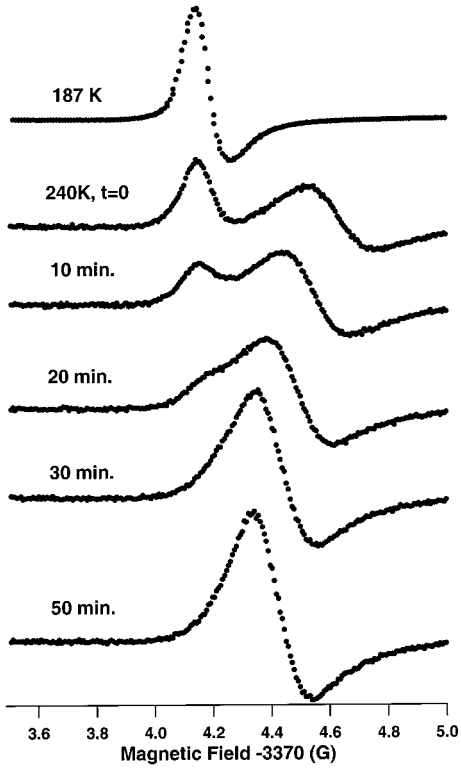

Figure 2. EPR spectra of $Cs^+(18C6)_2e^-$ during the transformation of a single crystal from the LT phase to the HT phase at a constant temperature of 240 K. The top spectrum is that of the initial pure LT phase at 187 K. Experimental conditions resulted in mixed absorption−dispersion mode spectra for both phases, which could be well fit by using Lorentzian line shapes.

The slow conversion of the LT phase to the HT phase was strikingly confirmed by following the EPR spectrum of a small single crystal as a function of time after increasing the temperature to 240 K. Figure 2 shows the change in shape and position of the EPR spectrum with time. All spectra could be quantitatively fit as a mixture of Lorentzian absorption and dispersion modes for the two phases (required because of the use of an external cavity to stabilize the frequency).

The temperature dependence of the ^{133}Cs NMR chemical shift, $\delta(T)$, is largely determined by the paramagnetic contact shift due to interaction with the electride electrons.[23] This will be referred to here as the Knight shift. The contact density at the cation nucleus, $|\psi(0)|^2$, is related to the Knight shift [$K(T)$] by

$$K(T) = \delta(T) - \delta(\infty) = \left(\frac{8\pi}{3N_{av}}\right)|\psi(0)|^2\chi(T) \qquad (1)$$

in which $\chi(T)$ is the electronic contribution to the magnetic susceptibility and all other symbols have their usual meanings.[37] Calculation of the contact density permits calculation of the fractional atomic character F by the equation

$$F = |\psi(0)|^2/|\psi(0)|^2_{atom} \qquad (2)$$

in which $|\psi(0)|^2_{atom}$ is the contact density of a gaseous atom, which for cesium is 2.645×10^{25} e cm^{-3}.[38] Since the susceptibility, which can be determined from the SQUID measurements, is proportional to $1/T$ for all phases in the temperature region over which NMR data are available, the chemical shift can be related to temperature through

$$\delta(T) = A/T + \delta(\infty) \qquad (3)$$

Figure 3 shows that the NMR data for all of the peaks follow the linear behavior predicted by eq 3. The chemical shift at infinite temperature, the Knight shift, the contact density and the fractional atomic character, calculated from linear least-squares fits of eq 3 to the data, combined with eqs 1 and 2 and the susceptibility data, are given in Table 1.

The Knight shift and fractional atomic character of the HT phase are in good agreement with the previously published measurements. However, the more complete temperature calibration used in the present study shows that the HT and HT2 phases have somewhat different contact densities, in contrast to the previously assumed constant value.[23] The chemical shifts previously found at the four calibrated temperatures agree well with those obtained in the present study, in which *all* temperatures were calibrated. Thus, although the details are slightly different, the major conclusion of the previous study[23] that the trapped electron density at the nucleus is extremely low is confirmed by this work; in fact, the contact density is very small for *all* the phases of this electride.

From the cavity-channel structure of this electride (to be described later) we expect crystalline $Cs^+(18C6)_2e^-$ to behave as a quasi-one-dimensional system. The spin anisotropy has been shown to be small[27] so the system should behave as an infinite isotropic (Heisenberg) chain. The spin Hamiltonian for such a system can be expressed (neglecting the Zeeman term) as

$$H = -2J\sum_i \hat{S}_i \cdot \hat{S}_{i+1} \qquad (4)$$

in which the coupling parameter J is negative for antiferromagnetic interactions. The published susceptibility of the carefully crystallized electride (never warmed above 230 K) shows a

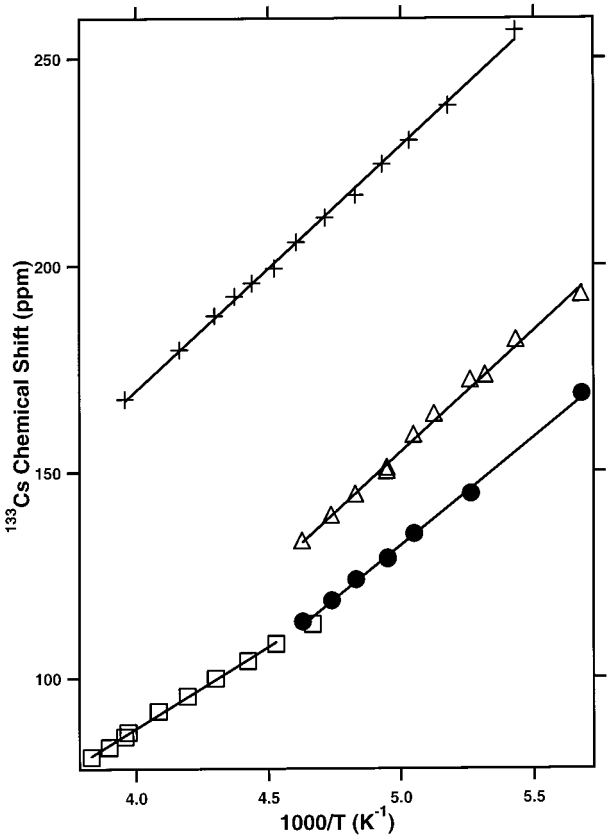

Figure 3. Temperature dependence of the NMR chemical shifts of various forms of $Cs^+(18C6)_2e^-$: LT peak (crosses), HT peak (squares), HT2a peak (filled circles), and HT2b peak (triangles). The linear least-squares fits by eq 3 are shown as solid lines, and yield the parameters given in Table 1.

TABLE 1: Parameters Obtained by Fitting Eq 3 and the Measured Magnetic Susceptibilities to the ^{133}Cs NMR Data

NMR peak	$\chi_m(T)$	$\delta(\infty)$ (ppm)	$10^{-4}K(T)T$ (ppm K)	$\lvert\psi(0)\rvert^2$	F
LT	1.37×10^{-3} ($T = 211$ K)	−67(3)[a]	5.92(7)	1.47×10^{22}	5.6×10^{-4}
HT	1.40×10^{-3} ($T = 239$ K)	−71(3)	3.98(7)	8.55×10^{21}	3.2×10^{-4}
HT2a	1.65×10^{-3} ($T = 206$ K)	−129(5)	5.2(1)	1.10×10^{22}	4.2×10^{-4}
HT2b	1.65×10^{-3} ($T = 206$ K)	−139(7)	5.9(1)	1.25×10^{22}	4.7×10^{-4}

[a] Numbers in parentheses are standard deviation estimates of the last digit.

broad maximum (see Figure 4) at about 50 K, indicating the presence of significant antiferromagnetic interactions.[28] While the temperature dependence of the susceptibility for a spin-$^1/_2$ linear chain Heisenberg antiferromagnet has not been solved as a closed form analytical expression, extrapolations of infinite chain behavior from finite size ring calculations have been published.[39] The results of these calculations have been fit by the convenient analytical expression

$$\chi_m = \frac{Ng^2\beta^2}{k_B T}\left[\frac{0.25 + 0.14995x + 0.30094x^2}{1 + 1.9862x + 0.68854x^2 + 6.0626x^3}\right] \quad (5)$$

in which $x = |J|/k_BT$.[40,41] Nonlinear least-squares fitting of the previously published data[28] by eq 5 resulted in the excellent fit shown in Figure 4, with $J/k_B = -38.3(1)$ K and 93.7(3)% of the expected number of spins. (Numbers in parentheses are

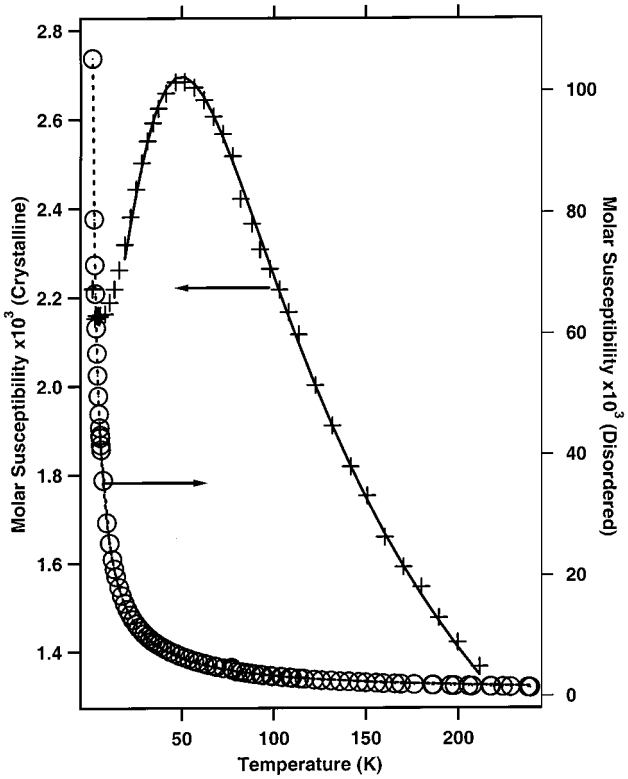

Figure 4. Molar magnetic susceptibility of the LT phase (crosses and left axis) and the HT phase (circles and right axis) of $Cs^+(18C6)_2e^-$. The solid line is the least-squares fit of eq 5 to the LT data while the dashed line is the fit of the Curie−Weiss equation to the HT data.

standard deviation estimates of the last digit.) The data used for the fit were truncated below 19 K; deviations from linear chain behavior occur at lower temperatures. These deviations might be due in part to the presence of some of the high-temperature phase that behaves as a Curie−Weiss paramagnet. However, this may not be the entire reason since addition of a Curie−Weiss term to eq 5 did not yield a good fit. Interchain coupling could also result in low temperature deviations, but the data could not be adequately fit by the addition of a mean field correction to eq 5. The presence of finite length chains may contribute a sub-Curie law term.[42] Of course, there may also be 3-D long-range ordering (a Néel transition) when zJ' (in which J' is the interchain coupling strength and z is the number of contributing neighbors) is comparable to kT.[43] Additionally, any finite spin anisotropy would split the parallel and perpendicular susceptibilities at sufficiently low temperatures.[39] Studies of single-crystal susceptibilities and magnetic heat capacity would be needed to resolve questions about the very low temperature behavior.

The HT phases show entirely different susceptibility behavior (Figure 4). The peak in the susceptibility is gone and the data are well described by the Curie−Weiss equation with $\theta = -2.3$ K and 90.6% spins as previously determined.[28] Such a dramatic change in behavior emphasizes the significant alteration of electron−electron interactions that accompany the LT to HT conversion.

The susceptibility behavior of the LT and HT phases was confirmed by EPR spin susceptibilities as shown in Figure 5. The data are somewhat scattered and the spin count could not be obtained because of the extremely small samples required to prevent loss of lock. Nevertheless, the presence of a maximum in the spin susceptibility of the LT phase ($J/k_B \sim -32$ K according to eq 5) and the Curie−Weiss behavior of the HT

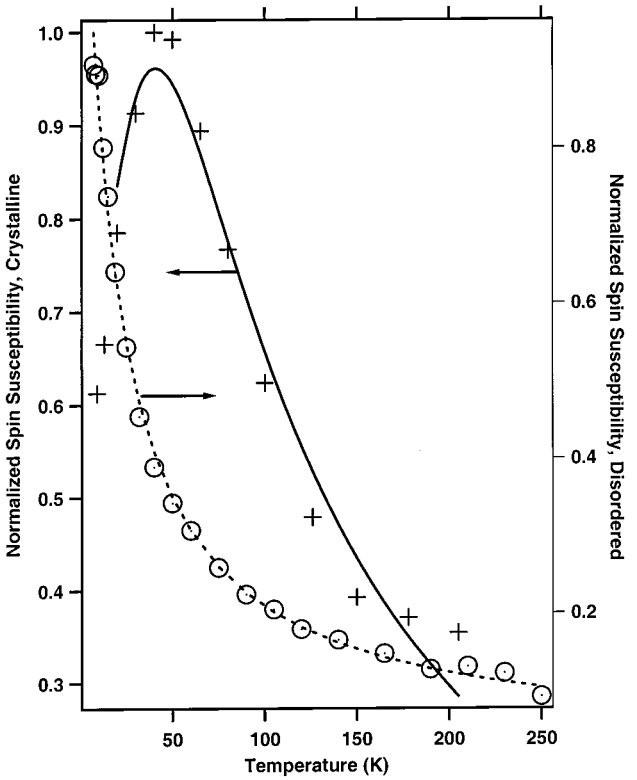

Figure 5. Normalized spin susceptibilities of powdered samples of the LT phase (crosses) and the HT phase (circles) obtained from EPR intensities as a function of temperature. The solid line is the least-squares fit of eq 5 to the LT data while the dashed line is the fit of the Curie−Weiss equation to the HT data.

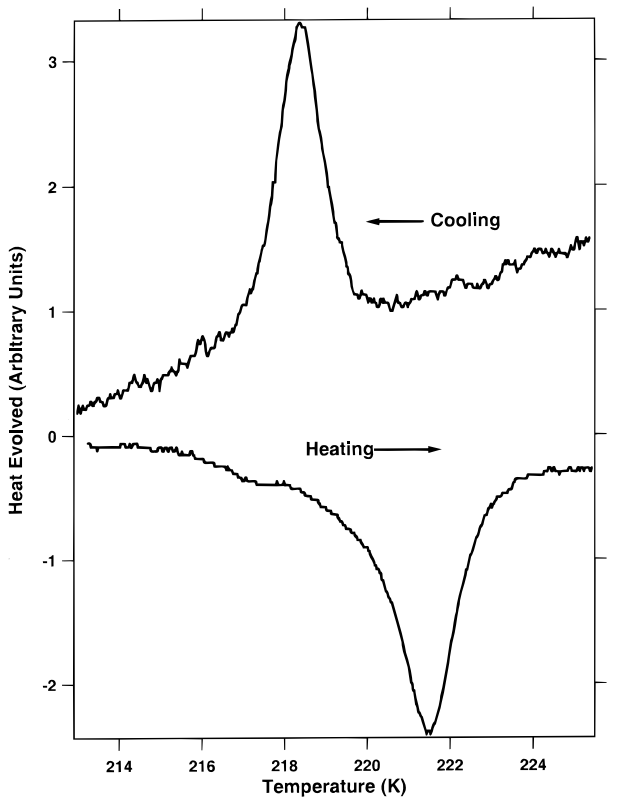

Figure 6. DSC scans of the high-temperature phase of $Cs^+(18C6)_2e^-$ that show the first-order "lattice melting" phase transition. At temperatures below this phase transition temperature, the ^{133}Cs NMR shows two peaks, designated HT2a and HT2b.

phase(s) ($\theta = -16$ K) agree qualitatively with the corresponding results from susceptibility measurements.

DSC measurements confirmed the reversible transition of the HT phase into the HT2 phase(s) seen in the NMR spectra. Upon warming the crystalline LT phase from 150 to 265 K, no enthalpy changes were observed. However, when the resulting HT phase was cooled, a small exotherm ($\Delta H = -0.21$ kJ mol^{-1}) appeared with an onset temperature of 219.7 K. Rewarming the sample resulted in the observation of an endotherm ($\Delta H = 0.33$ kJ mol^{-1}) with a gradual onset beginning at ~218 K (see Figure 6). The relatively larger magnitude of the endothermic enthalpy change (0.32 to 0.34 kJ mol^{-1}) compared to that of the exotherm (−0.21 to − 0.30 kJ mol^{-1}) was consistently observed upon repeated cycling, as expected for under-cooling.

A variable-temperature powder X-ray diffraction study was undertaken to assess the crystallinity of the HT phase. The diffraction patterns are shown in Figure 7. A freshly synthesized polycrystalline sample of the LT phase gave sharp lines at the positions expected from the known crystal structure. Repeated warming to ~240 K, which we know yields the HT phase, resulted in irreversible broadening of the peaks until only a few low-angle peaks were resolvable above an amorphous background. These remaining peaks were not compatible with the structure of the LT phase, but they indicate that some order remains upon conversion of the LT phase to the HT phase(s). They probably result from the remaining order of the Cs^+ ions, but this could not be confirmed. The remaining broad peaks do not necessarily mean that the HT phases are amorphous. Breakup into submicron crystallites would also give broad lines. There is some evidence from ^{133}Cs NMR studies (to be reported separately) that a crystalline HT2 phase exists.

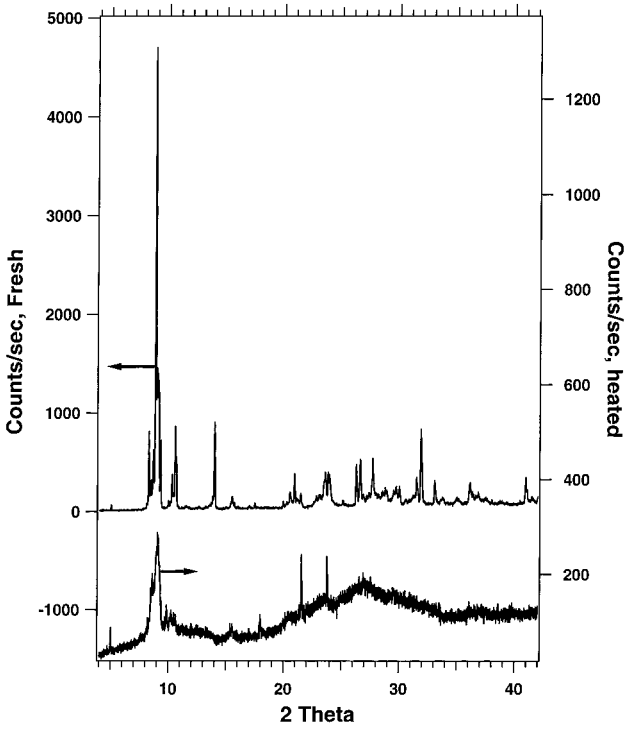

Figure 7. Powder X-ray spectra of polycrystalline $Cs^+(18C6)_2e^-$ at 190 K before (top and left) and after (bottom and right) heating three times to 240 K. The initial spectrum agrees with that predicted from the known crystal structure. Note the pronounced change in intensity that accompanies the phase transition.

The irreversible broadening of the X-ray powder pattern contrasts with the *reversible* X-ray powder patterns of alkalides that contain the complexant 15-crown-5.[44] Some of these

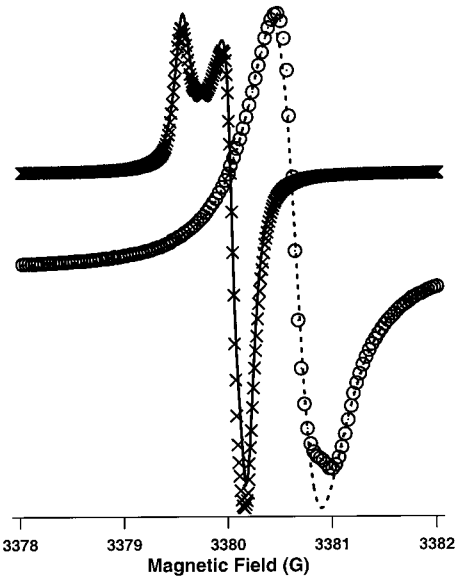

Figure 8. EPR spectra of powdered samples of the LT phase (crosses) at 125 K and the HT2 phase(s) (circles) of $Cs^+(18C6)_2e^-$ at 140 K. Lines through the data are least-squares fits to the appropriate equation (see text). Note that the two spectra were obtained at different microwave frequencies, 9.4715 GHz for the LT phase and 9.4746 GHz for the HT phase(s).

alkalide powder patterns also showed considerable line broadening above 230 K, probably as a result of complexant disorder, but the original pattern was restored when the temperature was decreased. [44]

A typical EPR spectrum of crushed crystals of the LT phase recorded at 125 K is shown in Figure 8. The fit of this spectrum by a rhombic **g**-tensor indicates that the electron trapping site is anisotropic. The fitting method employed a modification of the nonlinear least-squares program, KINFIT,[45] to vary the principle values of the **g** tensor, line width, and scaling factor until the sum of the squares of the residuals was a minimum. Although the shape of the spectrum is similar to that expected when only parallel and perpendicular components are present, a poorer fit to experiment was obtained with an axial **g** tensor. At other temperatures between 4 and 200 K, the EPR spectra of powdered samples of the LT phase were also well fit by using rhombic **g** tensors with similar principle values. Both the line width and the **g**-tensor components depend on temperature. The data are given in Table 2. Although individual uncertainties are not given, the estimated standard deviations at a particular temperature are generally less than 2 mG for the line width and 1×10^{-5} for the **g** values. As the temperature is increased from 3.7 K, the line width initially decreases and then increases linearly above 40 K. Interestingly, the g_{zz} value first increases and then decreases slowly above 12 K while the g_{xx} and g_{yy} components increase slightly with temperature. The ability to fit the EPR spectra to a single rhombic **g** tensor shows that all of the "anionic" electrons[8] in $Cs^+(18C6)_2e^-$ are trapped in equivalent sites in crystals of the LT phase, as expected from the crystal structure.

The saturation characteristics of the LT phase were similar to those obtained in an earlier study.[27] At a temperature below (3.7 K) and above (73 K) the maximum in the static susceptibility, the intensity of the signal initially increased linearly with the square root of the microwave power ($P^{1/2}$). The line width increased when the microwave power was greater than ~0.05 mW, as observed from the disappearance of the sharp signals from microcrystals into the underlying broad powder pattern spectrum. The line width and line shape differ noticeably at powers above 1 mW and an isotropic line shape results when $P > 100$ mW. Above 1 mW, the intensity deviates from linear $P^{1/2}$ behavior and increases only slowly thereafter. The signal never saturates completely but reaches a broad plateau of almost constant intensity that shows only slight downward curvature even at 440 mW of microwave power. These observations demonstrate substantial deviation from the usual saturation behavior of a single Lorentzian line.[46]

TABLE 2: Principal Values of the g-Tensor and Line Widths (ΔH_{pp}) Obtained by Fitting the Powder Pattern EPR Spectra of the Low-Temperature Phase to a Rhombic g-Tensor

T (K)	line width (mG)	g_{xx}	g_{yy}	g_{zz}
3.7	122	2.001 96	2.002 06	2.002 39
4.5	116	2.001 98	2.002 07	2.002 41
5.1	112	2.001 97	2.002 07	2.002 41
6.6	103	2.001 97	2.002 07	2.002 43
8.6	112	2.001 97	2.002 06	2.002 45
10.1	106	2.001 97	2.002 07	2.002 46
12	97	2.001 97	2.002 07	2.002 46
15	90	2.001 97	2.002 07	2.002 45
20	79	2.001 97	2.002 08	2.002 45
30	73	2.001 98	2.002 08	2.002 44
40	74	2.001 99	2.002 10	2.002 43
50	82	2.002 01	2.002 11	2.002 43
65	86	2.002 01	2.002 12	2.002 42
80	93	2.002 01	2.002 11	2.002 40
100	101	2.002 03	2.002 12	2.002 40
125	110	2.002 04	2.002 13	2.002 40
150	118	2.002 06	2.002 14	2.002 40
175	121	2.002 04	2.002 12	2.002 35

Because no deconvolution is required, the temperature-dependent behavior of a *single crystal* of the low-temperature phase permitted accurate determination of the intrinsic line width. In addition, the temperature variation of the single-crystal line width and intensity were qualitatively similar to those of the polycrystalline LT phase. Because of the difficulty of handling an extremely small crystal that is both temperature and air sensitive, the orientation of the crystal with respect to the laboratory field was not known. However, the measured g value, which increased from 2.002 16 at 4 K to 2.002 20 at 187 K, was within the range determined from the powder pattern spectra. In Figure 9, the normalized EPR intensity and line width of the LT phase single crystal are plotted as a function of temperature between 4 and 187 K. As indicated above, the use of an external cavity yielded line shapes that were a mixture of absorption and dispersion modes. As a result, the line widths and intensities were determined by simulation of the EPR spectrum. The relative amounts of absorption and dispersion were varied, with the same line width used for each. The overall magnitude of the EPR signal was calculated by taking the square root of the sum of the squares of the amplitudes of the absorption and dispersion lines. At the maximum of the signal intensity, near 25−30 K, the peak-to-peak line width is a minimum, 51 mG, while the maximum line width, 93 mG, is reached at 187 K. The satisfactory fit of the single-crystal EPR spectrum to a single Lorentzian line at each temperature again shows that the EPR spectrum of the LT phase is due to a single site that has a unique orientation with respect to the lab field.

Although the fits of the single-crystal spectra of the LT phase were in general satisfactory, at temperatures below 180 K very small deviations from a pure Lorentzian line shape were observed. When the modulation frequency was raised above 1.56 kHz, the line width increased, suggesting that the EPR spectra at low temperatures may exhibit the effects of rapid passage. The lowest modulation frequency available with our instrument is 1.56 kHz and still lower modulation frequencies

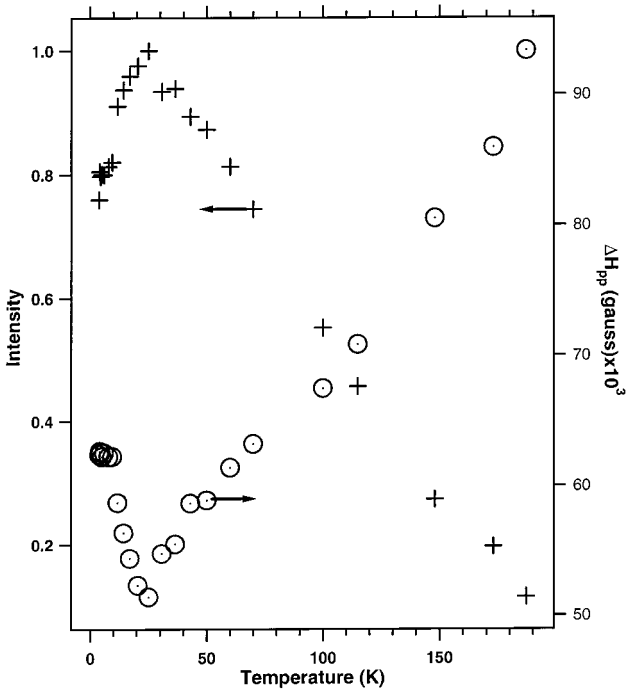

Figure 9. Intensity (plus signs and left axis) and line width (circles and right axis) of the EPR spectrum of a single crystal of the LT phase of $Cs^+(18C6)_2e^-$ as functions of temperature.

would help to verify the importance of passage effects on the EPR spectra of this and other electrides. It should be mentioned, however, that the fit of the single-crystal spectra to a Lorentzian was excellent above 180 K, showing that relaxation effects are sensitive to temperature. The powder pattern spectra suffered from an additional complication. In order to obtain a powder pattern spectrum that was not overwhelmed by signals from microcrystals, the size of the sample needed to be ~1−2 mg. However, this quantity of electride added a dispersive component to the EPR spectrum as evidenced by frequency shifts of up to 0.5 MHz when the resonance condition was reached. Some variation in microwave frequency was unavoidable for even the smallest samples, and, in combination with possible rapid passage effects, made precise simulations of the powder pattern spectra impossible.

As the temperature was raised above 210 K, two distinct EPR signals were observed, indicating that the single crystal had begun to convert from the low-temperature phase to the high-temperature phase. The variation of the EPR spectrum of a single crystal with time at 240 K is shown in Figure 2. The EPR signal due to the low-temperature phase is at lower field (higher g value). During the conversion, the spectra could be fit quantitatively by two Lorentzian lines, with both dispersion and absorption components for each line. The conversion to the high-temperature phase (without *apparent* disintegration of the crystal) was complete after ~50 min at 240 K. The bottom spectrum in Figure 2 is fit by a single Lorentzian line with dispersion and absorption components ($\Delta H_{pp} = 0.17$ G, $g =$ 2.00 206). This shows that at 240 K a single site (or rapid exchange between sites) is responsible for the EPR spectrum of the HT phase of the converted single crystal. However, a single Lorentzian line could *not* account for the EPR spectra of this sample at low temperatures. The sum of two Lorentzian lines with different g values and line widths provided a much better fit. This is consistent with the observation of two distinct NMR resonances below the 220 K phase transition of the HT samples as described above. The best-fit g values of the two components were essentially temperature independent, with a difference of $\Delta g = 4.2 \times 10^{-5}$ down to 4 K, while the line widths varied slowly with temperature. Although Δg is not large enough to observe two distinct peaks, the improved fits of the spectra of this converted single crystal give compelling evidence for at least two geometrically distinct electron-trapping sites in the low-temperature HT2 phase(s). As with powdered samples (Figure 5), the normalized EPR intensity of the HT phase(s), obtained by thermal conversion of a single crystal of the LT phase, showed Curie−Weiss temperature behavior, consistent with static susceptibility measurements on powders.[28]

The EPR spectrum of a *powdered* sample of the HT2 phase(s) at 140 K is shown in Figure 8. The sample used for this measurement was confirmed to consist of the HT2 phase(s) by ^{133}Cs MAS NMR spectroscopy. As described above, the spectrum of the HT2 phase(s) of the converted single crystal was attributed to contributions from two Lorentzian lines. Therefore, powdered samples were expected to require the superposition of two powder pattern spectra. But, because Δg is so small, there would be considerable overlap. Unsuccessful attempts to fit each spectrum with two Lorentzians (or to the pattern of a single rhombic site) indicate additional complications from unresolved g anisotropy. With these complications in mind, the EPR spectra were nevertheless fit with a single Lorentzian. As shown in Figure 8, the high-field part of the spectrum is not well fit. The best fits to Lorentzian line shapes yielded peak-to-peak line widths that increased from 0.43 G at 25 K to 0.53 G at 120 K and subsequently decreased at higher temperatures to a minimum value of 0.39 G at 250 K. The g value of 2.0024 was essentially independent of temperature. The variation of the EPR signal intensity between 4 and 250 K is shown in Figure 5 and affirms the Curie−Weiss behavior of the HT phase(s). Thus, although a quantitative treatment of the EPR spectra of HT phase powders was not possible, they are consistent with the results from other measurements.

The optical absorption spectrum of a vapor codeposited film at 211 K is shown in Figure 10 along with the spectrum of a film produced by evaporation of methylamine from a solution with the electride stoichiometry[47] and the reflectance spectrum from a single crystal. These spectra, with a distinct peak in the near-IR, are typical for an electride with localized electrons. As shown by the inset to Figure 10, the absorption peak shifts to lower energies as the temperature is increased, with a temperature coefficient of -3.1 cm^{-1} K^{-1}. As found previously for powders of this electride,[25] the vapor-deposited films were essentially insulating with $\sigma < 10^{-6}$ ohm^{-1} cm^{-1}. As with other alkalide and electride films,[48,49] thermionic electron emission currents in the picoampere range, presumably from defect sites, were observed with these films.

Discussion

The structure of $Cs^+(18C6)_2e^-$ (monoclinic space group $C2/c$) can be described as a close-packed arrangement of "expanded" cations with the charge balancing anions (electrons) occupying the vacancies left in the lattice. Each cesium cation is complexed by two 18-crown-6 complexant molecules in a sandwich fashion. While the expanded cations pack efficiently, they do leave considerable void space in the form of cavities and interconnecting channels.[10] The cavities are roughly elliptical in shape, being elongated down the c-axis. Adjacent cavities are connected together along the c-axis by a short, flat, open channel with an "hourglass" cross-sectional shape, about 1 Å by 4 Å in size. The center-to-center distance between cavities is 8.68 Å; however, since the cavities themselves are ap-

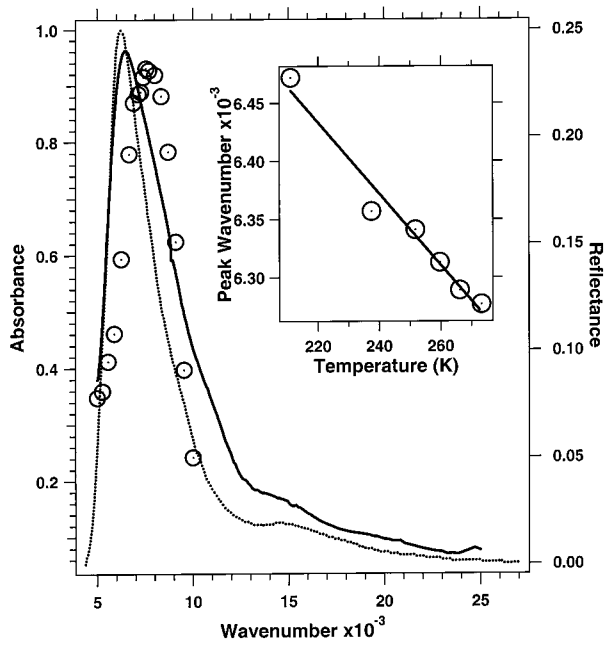

Figure 10. Absorbance (solid line and left axis) of a 2400 Å thick vapor codeposited film of $Cs^+(18C6)_2e^-$ and the normalized absorbance of a film produced by evaporation of methylamine from a solution of this stoichiometry (dotted line and left axis). Circles are the normal incidence reflectance (right axis) from a single crystal of the LT phase. The inset gives the temperature dependence of the absorption peak position of the vapor codeposited film.

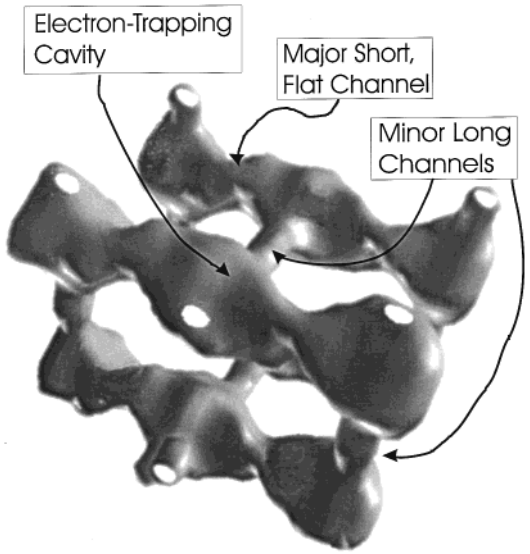

Figure 11. Cavity-channel geometry of the LT phase of $Cs^+(18\text{-Crown-}6)_2e^-$ obtained from the crystal structure. This surface represents the locus of points that lie 0.54 Å from the atomic van der Waals surfaces. The original picture[10] has been touched up to remove fragments from other chains and to show the continuations of the smaller longer channels (white circles).

proximately 7 Å in length, the effective channel length is less than 2 Å. Each cavity is also connected to four other cavities in the $a-b$ plane by longer channels with nearly circular cross sections. The center-to-center distance is 10.27 Å and the cavity radius is approximately 2 Å, so the effective channel length is more than 6 Å. These features can be seen in the depiction of the cavities and channels in Figure 11, which was constructed from the X-ray structural data.[10]

The cavity and channel structure can be used to develop a model of the magnetic interactions. Since the electrons are largely confined to lattice voids, the size and length of the interconnecting channels will determine the interactions of neighboring electrons. There is, in fact, a strong correlation between the cross-sectional area of the major channel in electrides and the interelectron coupling constant ($-J$).[12] The short channels along the *c*-axis provide much larger nonorthogonal overlap of neighboring electrons than the long channels in the $a-b$ plane, resulting in strong linear chain antiferromagnetic interactions.

It is clear that the magnetic susceptibility data for the LT phase are in accord with those expected from the cavity and channel structure. The coupling between nearest neighbors in the electron chains is *at least* eight times larger than that between the neighbors in the $a-b$ plane as one would expect from the much shorter and more open channels along the *c*-axis.

Previous studies have shown that the properties of $Cs^+(18C6)_2e^-$ are critically dependent on the method of synthesis and the thermal history of the sample. For example, it was shown that the EPR spectrum of the noncrystalline powder consisted of a single narrow line whose width was independent of temperature.[21] In addition, the line shape appeared Dysonian at higher temperatures, indicating high microwave conductivity. A later study employed both X-band and high-frequency (250 GHz) EPR and demonstrated the presence of two EPR signals in a powdered crystalline sample.[27] Since the X-band data at that time seemed to indicate that the EPR spectrum consisted of two isotropic Lorentzian lines, the conclusion was that two distinct trapping sites existed in the crystalline form of $Cs^+(18C6)_2e^-$. In view of the present study, which used freshly prepared electride of the LT phase with known structure, as well as samples that were unambiguously shown to be the HT phase, the X-band and 250 GHz data can be reinterpreted.

The later work at X-band[27] showed spectra similar to that of the LT phase displayed in Figure 8. At that time, the fit to an axial **g** tensor with $g_{\|} = 2.0024$ and $g_{\perp} = 2.0021$ was rejected in favor of the sum of two Lorentzian lines. Although the sum of two lines provided a better fit, this interpretation was less satisfactory because the cavity-channel picture based on the crystal structure shows that there should be only one electron trapping site in $Cs^+(18C6)_2e^-$. The fit to the axial **g** tensor may have been worse for two reasons: (1) The sample may have been a mixture of the LT and HT phases. (2) The spectrometer used in that study did not have the capability to discern the effects of rapid passage. The EPR spectra from the same batch of electride taken at 250 GHz (which may have had a different thermal history however) showed that two sites with different **g** tensors were needed to satisfactorily fit the observed spectrum. The best fit required an orientation dependent line width for both sites with axial **g** tensors, which for site one were $g_{\|} = 2.002\ 16$ and $g_{\perp} = 2.002\ 52$ and for site two $g_{\|} = 2.002\ 46$ and $g_{\perp} = 2.002\ 19$ at 158 K.

The present work shows that the LT and HT phases have different powder pattern EPR spectra. The *g* values of the LT phase are comparable to those determined for site two from the 250 GHz data and are very close to the values obtained from the previous study at X-band.[27] Therefore, the sample used for the high-frequency experiment was most likely a mixture of the LT and HT phases of $Cs^+(18C6)_2e^-$.

The anisotropy of the **g** tensor for the LT phase powder pattern and the presence of only a single Lorentzian line for a single crystal provide conclusive evidence for a single electron-trapping site that is anisotropic. This result is consistent with the "stoichiometric F-center" model of the electride in which

the electron-trapping site is an anisotropic cavity. The difference in EPR line width of the single crystal at 250 K after conversion to the HT phase (0.17 G) from that of the HT phase powder sample (0.39 G) suggests that the LT to HT conversion occurs with some retention of crystalline order.

Although the powder X-ray diffraction data indicate that the high-temperature phases are either disordered or microcrystalline, some conclusions about their general structural features can be drawn from the NMR data. The calculated chemical shifts at infinite temperature for both the LT and the HT phases agree well with those seen in $Cs^+(18C6)_2$ alkalides and in conventional salts.[23] The infinite temperature chemical shift is mainly determined by the Cs^+-O overlap. The conformations of the sandwiched cations must therefore be quite similar in the LT and HT phases. The 100 ppm difference in the chemical shifts of the LT and HT phases derives mainly from a decrease in the contact density at Cs^+ in the HT phase. The chemical shifts at infinite temperature of the two peaks of the HT2 phase(s) are the same within experimental error. However, they are diamagnetically shifted by 60−70 ppm from those of the LT and HT phases. This suggests weaker Cs^+-O overlap for the HT2 phase(s), with contact densities that are intermediate to those of the LT and HT phases. An alternative explanation of the more diamagnetic infinite temperature chemical shift of the HT2 phase(s) is that the fractional atomic character of the HT2 phase(s) might be temperature dependent, so that linear extrapolation vs $1/T$ to infinite temperature is not valid.

The previous NMR study[23] had found that the electride could be doped with sodium to make mixed electride−sodide systems. From the chemical shift range observed, these samples must have been in the HT phase. The ^{133}Cs spectra exhibited five peaks, one at the shift of the HT phase of the electride, one at the shift of the pure sodide, and three others that were spaced at intervals of $^1/_8$th of the distance between the peaks of the end members. These peaks were interpreted as being due to the successive substitution of the diamagnetic sodium anion into the cavities surrounding the complexed cesium cations, thus eliminating the interaction of one trapped electron (and hence its contribution to the Knight shift) for each substitution. This requires that each trapped electron in the HT phase contribute equally to the Knight shift; otherwise the peaks would not be equally spaced. Such an effect would not be expected for trapped electrons in the known crystal structure since the eight trapping sites that surround each complexed cation are at different distances from Cs^+. It seems unlikely that access to the cesium cation through the crown would coincidentally equalize the contact densities. The observed behavior of the sodium-doped HT phase of the electride implies that the transition from the LT to the HT phase involves both rearrangements of the complexed cations and complexant motion. The transition retains the Cs^+-O interaction, as indicated by the values of the chemical shift at infinite temperature, but in the HT phase the trapped electrons are at a more nearly equal *average* distance from the cation.

A model of the transition from the LT to the HT phase that is consistent with all the data is one in which the complexed cations rearrange from their uniformly canted rows in the crystal to a more randomly canted structure as a result of "lattice melting". It is known that crown ether molecules in the isostructural sodide undergo rapid "merry-go-round" reorientation in the temperature region in which the LT to HT transition is observed.[50,51] In the electride, motions about the cant angle might accompany rotation of the crown ether. Such a rearrangement would be a temperature-dependent second-order effect and thus would not be seen by DSC. Motion of the crown ether molecules may then be inhibited upon lattice freezing of the HT phase to form the HT2 phase(s), thus locking in the disorder. This would be consistent with the irreversible loss of order seen in the X-ray powder patterns. A detailed study of single crystals by ^{133}Cs NMR that relates the quadrupolar and chemical shift tensors to the crystal structure will be published separately.

The disorder that accompanies the LT to HT transition could also account for the observed change from quasi-one-dimensional antiferromagnetism to Curie−Weiss paramagnetism. It may result in two effects that would tend to minimize interelectron overlap; first, the cavities might be larger or more spherical in shape; second, the channels might be pinched off or lengthened.[28] One could think of the electrons in the LT phase as having some p character because of the elongated nature of the cavities, resulting in greater overlap of the wave functions along the channel axis. In the HT phase, either a more spherical cavity shape or blockage of the channels by the rearranged complexant molecules would decrease the overlap of neighboring electrons.

Within this model, a speculative description of the general structural features of the HT2 phase can be made. The substantial diamagnetic shift of the infinite temperature intercept that accompanies the transition from the HT to the HT2 phase could be accounted for by looser complexation in the latter phase. The isolation of the trapped electrons in the HT form must be retained since no discontinuity in the magnetic susceptibility is observed. However, the "lattice freezing" from the HT to the HT2 phase(s) results in a stronger average Cs^+-e^- overlap, perhaps due in part to a contraction of the lattice upon freezing. The HT2 phase may be related to that of $Cs^+(18C6)_2Cs^-$ between 230 and 285 K, which also displays two cation peaks in the ^{133}Cs NMR spectrum, separated by ∼10 ppm.[23] (No X-ray structural data are available for $Cs^+(18C6)_2Cs^-$ in this temperature range.)

The thermally induced transition from the LT phase to the HT phase does not answer all of the questions related to the differences between previous and more recent studies. Previous magnetic susceptibility studies found Curie−Weiss behavior[18,21,22] similar to that seen in the HT phases. However, a thermally induced transition to the HT phase could not be responsible for the low spin counts previously observed (never exceeding about 80% of the expected free spins). This behavior can be reproduced by recrystallizing the pure electride in the presence of a small percentage of $Cs^+(18C6)_2Cs^-$. Additionally, the larger conductivity of the ceside, compared to that of the electride,[25] could be resolved by the "ceside-doping" explanation. Ceside doping in the earlier studies but not in the present case is understandable since in the more recent studies, $Cs^+(18C6)_2e^-$ was synthesized in the presence of a slight excess of the complexant to drive the solution equilibrium

$$2Cs^+(18C6)_2e^- \rightleftarrows Cs^+(18C6)_2Cs^- + 2(18C6) \qquad (8)$$

to the left. Previously, the electride was typically made with stoichiometric solutions, which could have resulted in the inclusion of a small percentage of cesium in the lattice, formally as ceside.

The model of the phase changes presented above, while being consistent with all the experimental data, is admittedly speculative. These phase changes are intriguing and should alert the reader to the ease with which polymorphism can occur in molecular crystals such as alkalides and electrides. Such effects have also been observed in the electrides $Cs^+(15C5)_2e^-$ [52] and Li^+(cryptand[211])e^-.[53] However, the main purpose of this study

was to unambiguously establish the properties of the phase of $Cs^+(18C6)_2e^-$ that has the published crystal structure. It is clear that the magnetic properties are consistent with those expected from electrons confined to the cavities and channels in the structure, as has been found for other electrides.[10] In addition, measurement of the contact density at Cs^+ in the crystalline electride confirms that, while it is slightly higher than previously reported, it is still extraordinarily small and is consistent with virtual exclusion of the electride electron from the cesium core. So, while the $Cs^+(18C6)_2e^-$ system is much more complex and intriguing than previously thought, it can, in all its forms, still be called a "stochiometric F-center salt".

Acknowledgment. This research was supported by NSF Solid State Chemistry Grants DMR 94-02016 and DMR 96-10335 and by the Michigan State University Center for Fundamental Materials Research.

References and Notes

(1) Dye, J. L.; Ellaboudy, A. *Chem. Br.* **1984**, *20*, 210−215.
(2) Dye, J. L. *Prog. Inorg. Chem.* **1984**, *32*, 327−441.
(3) Dye, J. L.; DeBacker, M. G. *Annu. Rev. Phys. Chem.* **1987**, *38*, 271−301.
(4) Dye, J. L. *Sci. Am.* **1987**, *257*, 66−75.
(5) Dye, J. L. *Science* **1990**, *247*, 663−668.
(6) Dye, J. L.; Huang, R. H. *Chem. Br.* **1990**, *26*, 239−244.
(7) Wagner, M. J.; Dye, J. L. *Annu. Rev. Mater. Sci.* **1993**, *23*, 223−253.
(8) Dye, J. L. *Nature* **1993**, *365*, 10−11.
(9) Dye, J. L. *Chemtracts—Inorg. Chem.* **1993**, *5*, 243−270.
(10) Dye, J. L.; Wagner, M. J.; Overney, G.; Huang, R. H.; Nagy, T. F.; Tomanek, D. *J. Am. Chem. Soc.* **1996**, *118*, 7329−7336.
(11) Wagner, M. J.; Dye, J. L. In *Molecular Recognition: Receptors for Cationic Guests*, 1st ed.; Gokel, G. W., Ed.; Pergamon Press: Oxford, UK, 1996; Vol. 1, pp 477−510.
(12) Dye, J. L. *Inorg. Chem.* **1997**, *36*, 3816−3826.
(13) Allan, G.; DeBacker, M. G.; Lannoo, M.; Lefebvre, J. *Europhys. Lett.* **1990**, *11*, 49−53.
(14) Rencsok, R.; Kaplan, T. A.; Harrison, J. F. *J. Chem. Phys.* **1990**, *93*, 5875−5882.
(15) Singh, D. J.; Krakauer, H.; Haas, C.; Pickett, W. E. *Nature* **1993**, *365*, 39−42.
(16) Rencsok, R.; Kaplan, T. A.; Harrison, J. F. *J. Chem. Phys.* **1993**, *98*, 9758−9764.
(17) Rencsok, R.; Jackson, K. A.; Kaplan, T. A.; Harrison, J. F.; Pederson, M. R. *Chem. Phys. Lett.* **1996**, *262*, 207−212.
(18) Dawes, S. B.; Ward, D. L.; Huang, R. H.; Dye, J. L. *J. Am. Chem. Soc.* **1986**, *108*, 3534−3535.
(19) Ellaboudy, A.; Dye, J. L.; Smith, P. B. *J. Am. Chem. Soc.* **1983**, *105*, 6490−6491.
(20) Ellaboudy, A. Ph.D. Dissertation, Michigan State University, East Lansing, MI, 1984.
(21) Issa, D.; Ellaboudy, A.; Janakiraman, R.; Dye, J. L. *J. Phys. Chem.* **1984**, *88*, 3847−3851.
(22) Dawes, S. B. Ph.D. Dissertation, Michigan State University, East Lansing, MI, 1986.
(23) Dawes, S. B.; Ellaboudy, A. S.; Dye, J. L. *J. Am. Chem. Soc.* **1987**, *109*, 3508−3513.
(24) Moeggenborg, K. J. Ph.D. Dissertation, Michigan State University, East Lansing, MI, 1990.
(25) Moeggenborg, K. J.; Papaioannou, J.; Dye, J. L. *Chem. Mater.* **1991**, *3*, 514−520.
(26) Shin, D. H. Ph.D. Dissertation, Michigan State University, East Lansing, MI, 1992.
(27) Shin, D. H.; Dye, J. L.; Budil, D. E.; Earle, K. A.; Freed, J. H. *J. Phys. Chem.* **1993**, *97*, 1213−1219.
(28) Wagner, M. J.; Huang, R. H.; Dye, J. L. *J. Phys. Chem.* **1993**, *97*, 3982−3984.
(29) Dye, J. L. *J. Phys. Chem.* **1984**, *88*, 3842−3846.
(30) Dawes, S. B.; Ward, D. L.; Fussa-Rydel, O.; Huang, R.-H.; Dye, J. L. *Inorg. Chem.* **1989**, *28*, 2132−2136.
(31) English, A. D. *J. Magn. Reson.* **1984**, *57*, 491−493.
(32) Jaenicke, S.; Faber, M. K.; Dye, J. L.; Pratt, W. P., Jr. *J. Solid State Chem.* **1987**, *68*, 239−246.
(33) Skowyra, J. B.; Dye, J. L.; Pratt, W. P., Jr. *Rev. Sci. Instrum.* **1989**, *60*, 2666−2672.
(34) Hendrickson, J. E.; Kuo, C. T.; Xie, Q.; Pratt, W. P., Jr.; Dye, J. L. *J. Phys. Chem.* **1996**, *100*, 3395−3401.
(35) Hendrickson, J. E.; Pratt, W. P., Jr.; Phillips, R. C.; Dye, J. L. *J. Phys. Chem. B* **1998**, *102*, 3917−3926.
(36) A statement to the contrary[28] was incorrect.
(37) Knight, W. D. *Phys. Rev.* **1944**, *76*, 1259−1260.
(38) Edwards, P. P. *Adv. Inorg. Chem. RadioChem.* **1982**, *25*, 135−182.
(39) Bonner, J. C.; Fisher, M. E. *Phys. Rev. A* **1964**, *135*, 640−658.
(40) Estes, W. E.; Gavel, D. P.; Hatfield, W. E.; Hodgson, D. *Inorg. Chem.* **1978**, *17*, 1415−1421.
(41) Hall, J. W. Ph.D. Dissertation, University of North Carolina, Chapel Hill, 1977.
(42) Soos, Z. G.; Bondeson, S. R. *Mol. Cryst. Liq. Cryst.* **1982**, *85*, 19−31.
(43) Bonner, J. C. In *Magneto-Structural Correlations in Exchange Coupled Systems*; Willet, R. D., et al., Eds.; D. Reidel Publishing Co.: Dordrecht, Holland, 1985; pp 157−205.
(44) Doueff, S.; Tsai, K.-L.; Dye, J. L. *Inorg. Chem.* **1991**, *30*, 849−851.
(45) Nicely, V. A.; Dye, J. L. *J. Chem. Educ.* **1971**, *48*, 443−448.
(46) Poole, C. P. J. *Electron Spin Resonance*; Wiley-Interscience: New York, 1967; pp 705−710.
(47) Dye, J. L.; DaGue, M. G.; Yemen, M. R.; Landers, J. S.; Lewis, H. L. *J. Phys. Chem.* **1980**, *84*, 1096−1103.
(48) Huang, R. H.; Dye, J. L. *Chem. Phys. Lett.* **1990**, *166*, 133−136.
(49) Phillips, R. C.; Dye, J. L., unpublished results, this laboratory, 1999.
(50) Wagner, M. J.; McMills, L. E. H.; Ellaboudy, A. S.; Eglin, J. L.; Dye, J. L.; Edwards, P. P.; Pyper, N. C. *J. Phys. Chem.* **1992**, *96*, 9656−9660.
(51) Ratcliff, C. I.; Ripmeester, J. A.; Buchanan, G. W.; Denike, J. K. *J. Am. Chem. Soc.* **1992**, *114*, 3294−3299.
(52) Dawes, S. B.; Eglin, J. L.; Moeggenborg, K. J.; Kim, J.; Dye, J. L. *J. Am. Chem. Soc.* **1991**, *113*, 1605−1609.
(53) Huang, R. H.; Wagner, M. J.; Gilbert, D. J.; Reidy-Cedergren, K. A.; Ward, D. L.; Faber, M. K.; Dye, J. L. *J. Am. Chem. Soc.* **1997**, *119*, 3765−3772.